Taylor & Francis
Taylor & Francis Group

Check for updates

Energy optimal point-to-point motion profile optimization

Nick Van Oosterwyck[a,d], Foeke Vanbecelaere[b,e#], Ferre Knaepkens[c], Michael Monte[b,e], Kurt Stockman[b,e], Annie Cuyt[c,f], and Stijn Derammelaere[a,d]

[a]Department of Electromechanics, Cosys-Lab, University of Antwerp, Antwerp, Belgium; [b]Department of Electrical Energy, Metals, Mechanical Constructions and Systems, Ghent University campus Kortrijk, Kortrijk, Belgium; [c]Department of Mathematics and Computer Science, University of Antwerp, Antwerpen, Belgium; [d]AnSyMo/Cosys, Flanders Make, the Strategic Research Center for the Manufacturing Industry, Lommel, Belgium; [e]FlandersMake@UGent–Core Lab EEDT-MP, Ghent, Belgium; [f]College of Mathematics and Statistics, Shenzhen University Shenzhen, Guangdong, China

ABSTRACT

Position-controlled systems driving repetitive tasks are of significant importance in industrial machinery. The electric actuators used in these systems are responsible for a large part of the global energy consumption, indicating that major savings can be made in this field. In this context, motion profile optimization is a very cost-effective solution as it allows for more energy-efficient machines without additional hardware investments or adaptions. In particular, mono-actuated mechanisms with position-dependent system properties have received considerable attention in literature. However, the current state-of-the-art methods often use unbounded design parameters to describe the motion profile. This both increases the computational complexity and hampers the search for a global optimum. In this paper, Chebyshev polynomials are used to describe the motion profile. Moreover, the exact bounds on the Chebyshev design parameters are derived. This both seriously reduces the computational complexity and limits the design space, allowing the application of a global optimizer such as the genetic algorithm. Experiments validate the added value of the chosen approach. In this study, it is found that the energy consumption can be reduced by 62.9% compared to a standard reference motion profile.

1. Introduction

In the last decades, economic considerations and stricter government regulations have driven engineers to come up with new techniques to reduce the energy consumption of industrial machinery. Statistics indicate that electric motors are generally responsible for about 2/3 of the industrial electricity consumption, which indicates that major savings are to be made in this field (Bo, 2008).

In this context, several technologies and methods have been developed to reduce the electrical energy consumption of mechatronic systems. For instance, (Glodde and Afrough, 2014) has demonstrated that replacing machinery with existing well-established energy-efficient technologies
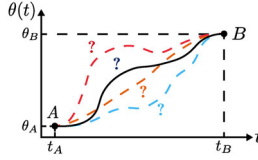

Figure 1. Motion profile of a PTP movement with constraints θ_A, θ_B, t_A and t_B.

results in savings of approximately 57%. Nevertheless, the acquisition of new equipment entails certain costs, which hampers the wide spread of these innovations.

Motion profile optimization on the other hand, is a cost-effective alternative which can be implemented without additional investments in hardware. It starts from the idea that in many industrial applications, only part of the motion is constrained by the process requirements. Hence, an optimization potential rises in the non-constrained part of the position function $\theta(t)$, in between the start $\theta(t_A) = \theta_A$ and endpoint $\theta(t_B) = \theta_B$ of the point-to-point (PTP) motion (Figure 1). Moreover, since many industrial applications involve repetitive movements, the motion profile optimization effect will be perceptible every machine cycle, thus, making it an indispensable step in modern energy-efficient machine design. Therefore, in this paper, a motion profile optimization approach is presented which considers the motion profile $\theta(t)$ as a design variable in order to minimize the root-mean-square torque τ_{rms} and associated energy consumption E, while taking into account the motion requirement constraints of a rest-to-rest motion.

In the past literature, several motion profile optimization techniques have been proposed for multiple applications. An overview of possible approaches is covered in (Carabin et al., 2017) and (Rao, 2014). In general, the current techniques can be classified based on *application type*, *system property identification*, *optimization algorithm* and *motion profile function* $\theta(t)$.

As for the *application type*, a vast amount of research is focused on the optimization of conventional industrial robots (IRs) such as a 6-DOF serial robotic arm. For example, recent literature (Wu et al., 2022) proved that asymmetric jerk profiles can be used as an effective tool for the trajectories planning of IRs. Moreover, (Gadaleta et al., 2019) presented an optimization approach which interfaces with current robot offline programming tools used in industrial practices. However, these type of robots are specifically designed to work in flexible production environments and are, due to the 6 axis drive system mass, not suitable for those manufacturing environments where very high dynamics and accuracy are of utmost importance.

Therefore, lots of mechatronic systems are designed as rod mechanisms with a dedicated actuator. Given the tendency to evolve from a monoactuator driving all machine components toward dedicated positioners for each machine movement (Berselli et al., 2016), it is evident that one machine can contain numerous motion profile optimization opportunities where each axis is optimized independently. In (Richiedei and Trevisani, 2016), various motion profiles were compared for mechanical systems with constant load parameters such as the inertia J. In (Carabin and Vidoni, 2021), an analytic methodology is is developed for 1-DOF systems moving a constant inertia load. However, as indicated in literature (Pellicciari, Berselli, and Balugani, 2015), it is essential to consider varying loads to cover the majority of machine applications, which is also the focus of the present study.

For what concerns the *system property identification* approach, one can distinguish either analytic, CAD-based or online approaches. Analytic identification used in (Hsu et al., 2014) and (Ha et al., 2006) applies Hamilton's principle and Lagrange multipliers to obtain the differential-algebraic equations of the system. In (Sollmann et al., 2010), a method of virtual work is described to obtain the system matrix while (Vanbecelaere et al., 2020) determines the inertia profile using the method of kinetic energy. In (Brancati et al., 2007), analytic equations were derived for a two-link flexible manipulator. However, these analytic approaches are cumbersome, complex, error-prone, and are not easily applicable in industry. Especially given the trend indicated in (Walsch

et al., 2014) that there is a demand for methods that take into account the ease of implementation.

Fortunately, machine builders often already design their machines in 3 D CAD multibody software, which can be used to extract crucial information. Hence, in (Van Oosterwyck et al., 2019), the authors of this paper describe a technique to derive the position dependency of critical parameters inertia $J(\theta)$ and load torque $\tau_l(\theta)$, based on only three CAD motion simulations. The latter is also utilized in this paper. Similarly, if no CAD data is available, one can resort to online estimation techniques as described in (Vanbecelaere et al., 2022) and (Delchev and Zahariev, 2008).

As for *optimization algorithms*, the motion profile optimization problem can be regarded as an optimal control problem where the goal is not to determine an optimal control law, but instead, the aim is to optimize the path of the state, being the design parameter, to minimize the torque input which is this case is the objective. If optimal control problems are considered, several approaches are possible: dynamic programming, indirect methods and direct methods (Diehl et al., 2006).

On the one hand, dynamic programming can be used to solve unconstrained low-dimensional problems, but it does not scale well to high-dimensional systems and is computationally expensive due to the curse of dimensionality (Kelly, 2017).

On the other hand, (Park, 1996) and (Shiller, 1996) use an indirect approach such as Pontryagin's Maximum Principle to obtain the best possible control. However, this method tends to be abandoned recently (Chettibi et al., 2004) due to the difficulties of incorporating constraints and the fact that the underlying differential equations are often difficult to solve due to strong nonlinearity (Diehl et al., 2006).

Finally, direct approaches recast the optimization into a nonlinear programming problem (NLP), which can be solved with various numerical methods. In particular, (Gasparetto and Zanotto, 2007) and (Pellicciari, Berselli, and Balugani, 2015) use gradient-based methods such as Sequential Quadratic Programming (SQP) that are known to have very low solve times and good scalability. However, these algorithms can only deliver local optimal solutions and are not suited for problems with multiple minima. Moreover, as indicated in (Huang et al., 2018), the optimum obtained with gradient-based methods is greatly influenced by the selected starting points, which are to be chosen arbitrarily.

To avoid this problem, heuristic optimization algorithms such as generalized pattern search (GPS) (Gadaleta et al., 2019) or genetic algorithms (GA) (Van Oosterwyck et al., 2019) are of interest. In contrast to gradient-based algorithms that do not search the entire design space of the NLP problem, derivative-free algorithms like GA often sample a wide part of the search space in order to be successful (Wenzhong and Porandla, 2005). Hence, it is important to select a suited motion profile definition which allows to limit the design space and increases the chance of finding the global optimum. Nevertheless, because these heuristic solvers do not exploit gradient information, they are not computationally competitive with gradient-based methods (Betts, 1998). In this paper, both a gradient-based and heuristic genetic algorithm are used to assess the tradeoff between computational effort and global optimality.

Regarding the *motion profile function*, several papers rely on piecewise position functions, where either cubic (Baggetta et al., 2021), quintic (Kuenzer and Husty, 2016), or trigonometric (Nguyen et al., 2007) splines are used. However, the objective functions in these works, are characterized by many local minima, causing the risk of getting stuck in a suboptimal solution. For instance, in (Piazzi and Visioli, 1998), the usage of cubic splines resulted in a savings difference of 18% between the global and local optimum. Yet, only time-optimal motion profiles were considered. Moreover, in (Biagiotti and Melchiorri, 2021) it is emphasized that for the optimization problem using splines, the global optimum is not guaranteed and is undiscovered in some optimization cases. In (Carabin and Scalera, 2020) and (Cheng et al., 2021), trapezoidal and cycloidal speed profiles are compared. However, as these motion profiles are defined by the time and

position constraints, they only allow to optimize the intermediate time instances without actually altering the position function itself.

Finally, continuous motion profile functions such as classic polynomials (Lee and Ha, 2020) are also popular because they do not introduce high jerk peaks into the system, which increases the wear of the components. In (Boscariol et al. 2020), third and fifth-order polynomials are used to describe the motion profile of the end-effector, yet only for functionally redundant mechanisms. (Boryga and Graboś 2009) also employs polynomials but only considers an acceleration constraint without looking at the energy consumption. Moreover, the resulting polynomial optimization problem is known to be badly conditioned. For example in (Van Oosterwyck et al. 2019), the polynomial coefficients reached values up to $1.8 \ 10^{20}$.

To overcome this issue, the authors of this paper propose to use Chebyshev polynomials. The Chebyshev polynomials were introduced in (Vlassenbroeck and Van Dooren 1988) and (Mezzadri and Galligani 2016) for solving generic optimal control problems. This is thanks to their orthogonal properties and important advantages regarding numerical analysis. However, contrary to the present paper, (Vlassenbroeck and Van Dooren 1988) and (Mezzadri and Galligani 2016) also approximate the system behavior with Chebyshev polynomials to limit the computational cost of the optimization for a generic optimal control problem. Moreover, to the authors knowledge, no exact bounds on the coefficients of the Chebyshev polynomials have been derived before, which is crucial for limiting the design space and reducing the chance of failing to identify the global minimum.

Recently, a Cheyshev based motion profile optimization routine has been presented by the authors in (Van Oosterwyck et al. 2020). However, due to the numerous symbolic calculations involved in constructing the objective function, solve times of almost 2 hours were reported. In addition, the solutions in (Van Oosterwyck et al. 2020) were obtained using gradient-based solvers which have a high risk of getting stuck in local minima. Finally, only theoretical reductions were reported, thus, leaving the feasibility of the proposed motion profiles undetermined. This paper builds upon these previous results by providing five critical improvements:

- In order to reduce the computational burden, a discrete approach is presented which eliminates the use of symbolic operations. To do so, the discrete system property data which originates from the CAD motion simulations have to be properly rescaled and interpolated.
- As an accurate model of the system dynamics is crucial for a correct optimization, the dynamics of the mechanism are extended by including damping and friction into the optimization routine. In addition, a new identification procedure is described which is validated on an industrial case.
- A derivation for exact bounds of the Chebyshev polynomial coefficients is introduced. This allows limiting the feasible design space. The latter is an essential novelty of this paper as it reduces the computational time of the heuristic optimizer and increases the chance that the global optimum is revealed.
- To check the robustness of the proposed method against getting stuck in local optima, the resulting optimization problem is solved with both a fast gradient-based and a global heuristic solver (i.e. GA).
- Experimental tests have been carried out on an industrial pick-and-place unit to quantify the actual energy savings and check the feasibility of the optimized motion profiles.

2. System modeling

The complete mechatronic system can be divided into two subsystems (Figure 2). On the one hand, there is the *mechanical subsystem* which describes the dynamics of a generic single-axis system. For high dynamical applications, these systems usually consist of slider-crank mechanisms
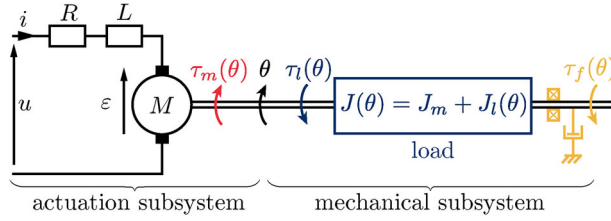
Figure 2. Schematic of the q-axis of a single axis mechanism.

and four-bar linkages (Berselli et al. 2016). Nevertheless, the approach is valid to any position-controlled system where the mechanism is driven by a single actuator.

On the other hand, there is the *actuation subsystem* which converts the electrical energy into mechanical energy and drives the mechanism. For the envisaged position-controlled systems, PMSMs are becoming the industry standard for rotary applications, whereas linear motors are used for fast and precise linear movements (Kiel 2008). In Figure 2, the PMSM actuator is represented by an equivalent DC model.

2.1. Mechanical subsystem

The dynamics of a single axis DOF mechanism can be described by means of the torque equation (Dresig and Holzweißig 2010):

$$\tau_m(t) = \tau_l(\theta) + \underbrace{J(\theta)\ddot{\theta}}_{\tau_a} + \underbrace{\frac{1}{2}\frac{\mathrm{d}J(\theta)}{\mathrm{d}\theta}(\dot{\theta})^2}_{\tau_v} + \tau_f(\dot{\theta}) \ . \tag{1}$$

With reference to Figure 2 and Equation (1), let us define $\theta = \theta(t)$ as the Lagrangian coordinate which describes the angular position of the main driving axis as a function of time t. The motor torque $\tau_m(t)$ is defined as the driving torque generated by the motor. The load torque $\tau_l(\theta)$ contains both gravitational forces as well as external process powers that act on the mechanism.

Furthermore, all inertias of the mechanism's components are related to the main driving axis resorting to the concept of reduced moment of inertia. Therefore, the reduced inertia of the complete system $J(\theta)$ is defined as a combination of the reduced load inertia $J_l(\theta)$ and inertia of the motor shaft itself J_m. Note that the position-dependent inertia of the system $J(\theta)$, results in two torque components when it is reduced to the motor side. The acceleration torque τ_a represents the part of the motor torque responsible for the motor acceleration forces that arise during the movement, while the variation torque τ_v compensates for the variation of inertia in the system.

Finally, the frictional torque $\tau_f(\dot{\theta})$ is defined as the result of frictional forces such as, for instance, viscous brush friction or dry bearing friction in the motor bearings and mechanical system. A commonly used model of friction shows three components of force: Coulomb (sliding) friction, viscous damping, and static friction (Ellis 2012). Regarding the PMSM, as indicated in (Westphal 2001, 175), the only appreciable friction effect in operation is viscous friction. Thus, coulomb and static frictions can be neglected in the PMSM model. For what concerns the mechanical model, only the viscous damping is modeled since the other friction components are constant and will not have an effect on the optimal motion profile:

$$\tau_f(\dot{\theta}) = \mu_v\dot{\theta} \ , \tag{2}$$

with μ_v the equivalent viscous friction coefficient.

The key benefit of the formulation in (1) is that it permits to model every possible mechanism with a known geometry and allows to define a generic optimization approach.

2.2. Actuation subsystem

Concerning the dynamics of the PMSM as depicted in Figure 2 (represented by an equivalent DC model), the electromechanical behavior can be easily described by the following basic laws (Rizzoni and Kearns 2003, 843):

$$\tau_m = k_t i \ , \tag{3}$$

$$u = Ri + L\frac{di}{dt} + \epsilon = Ri + L\frac{di}{dt} + pk_v\dot{\theta} \ , \tag{4}$$

with electric back emf ϵ, resistance R, back emf constant k_v, motor torque constant k_t, and number of pole pairs p, which can be found in the motor data sheet.

In what follows (4), the voltage drop $L\frac{di}{dt}$ due to the armature inductance is omitted as the mean value of its reactive power will be zero and therefore does not contribute to the system's energy need (Pellicciari, Berselli, and Balugani 2015).

Depending on whether the electric power flows from the drive unit to the PMSM's or vice versa, the PMSM operates in respectively motor or generator mode. In this latter condition, depending on the capabilities of the drive unit, the generated electric power can be either stored in a capacitor, dissipated as heat on a braking resistance, or transferred back to the energy source. Recent commercial PMSM drives are sized so that no electric power is actually dissipated during normal functioning so that the braking resistance is actually activated only under emergency conditions (Berselli et al. 2016). Therefore, in what follows, it is assumed that all the generated energy is returned to the grid and no losses occur in the process.

For a correct model of the actuation subsystem and prediction of the energy usage, it is important to model other losses such as cooling fans and drive circuitry as well. Nevertheless, the power consumption of these devices is generally considered constant and is therefore not affected by the motion profile (Gadaleta, Pellicciari, and Berselli 2019).

In order to minimize the total energy need E of the application, it is crucial to quantify the input energy of the complete system. Therefore, similar to (Berselli et al. 2016), a formulation of the input electrical energy E is derived and a torque-based design objective is obtained which allows to minimize the energy solely based on the mechanical parameters.

Starting from Equations (3) and (4), the instantaneous power P_e is defined as

$$P_e = u \ i = \frac{R}{k_t^2}\tau_m^2 + \frac{pk_v}{k_t}\tau_m\dot{\theta} \ . \tag{5}$$

The motion profile is defined on the time interval $t \in [t_A, t_B]$ and must have zero initial and final speed and acceleration, i.e. $\dot{\theta}(t_A) = \dot{\theta}(t_B) = \ddot{\theta}(t_A) = \ddot{\theta}(t_B) = 0$. Thus, the total energy can be expressed as

$$E = \int_{t_A}^{t_B} P_e \ dt = \int_{t_A}^{t_B} \left[\frac{R}{k_t^2}\tau_m^2 + \frac{pk_v}{k_t}\tau_m\dot{\theta}\right] \ dt \ . \tag{6}$$

Then, by incorporating the torque equation from (1), the total energy of the motion is given by:

$$E = \underbrace{\frac{pk_v}{k_t}\int_{t_A}^{t_B}(\tau_a + \tau_v)\dot{\theta} \ dt}_{E_k} + \underbrace{\frac{pk_v}{k_t}\int_{t_A}^{t_B}\tau_l \ \dot{\theta} \ dt}_{E_p} + \underbrace{\int_{t_A}^{t_B}\left[\frac{R}{k_t^2}\tau_m^2 + \frac{pk_v}{k_t}\tau_f\dot{\theta}\right]dt}_{E_l} \ . \tag{7}$$
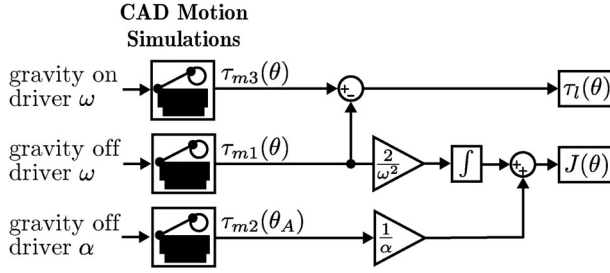
Figure 3. Schematic overview of the procedure for extracting position-dependent properties $J(\theta)$ and $\tau_l(\theta)$ based on three different CAD motion simulations (Van Oosterwyck et al. 2019).

Here, the first term E_k represents the kinetic energy of the moving masses in the system. Due to the rest-to-rest motion of the envisaged applications, this term reduces to zero. Further, the term E_p represents the potential energy stored in the system. As this term E_p only depends on the fixed start θ_A and end position θ_B, it is disregarded in the optimization routine (Berselli et al. 2016). The final term E_l represents the energy that is lost due to the coil resistance and frictional forces and is the only term that is affected by optimizing the motion profile $\theta(t)$. Nevertheless, in many industrial applications, the frictional forces τ_f are negligible (Park, 1996), especially if the inertial loads are predominant. Thus, the energy losses E_l can be expressed as:

$$E_l = \int_{t_A}^{t_B} \frac{R}{k_t^2} \tau_m^2 \mathrm{d}t = \frac{R\Delta t}{k_t^2} \tau_{rms}^2, \tag{8}$$

where τ_{rms} is the root-mean-square (RMS) value of the motor torque τ_m. This proves that the RMS torque τ_{rms} can be effectively used as an optimization objective to minimize the total energy usage of the system. This is very useful in situations where the motor coil properties are unknown or parameters are missing (Berselli et al. 2016).

3. Identification

3.1. Inertia and load torque

Identification of all the position varying parameters in the highly nonlinear differential torque Equation (1) is not straightforward. Fortunately, machine builders design their machines in 3D CAD multibody software. For this reason, (Berselli et al. 2016) and (Van Oosterwyck et al. 2019) describe a technique to derive the position dependency of critical parameters inertia $J(\theta)$ and load torque $\tau_l(\theta)$, based on three CAD motion simulations (Figure 3).

In this paper, the identification routine is illustrated by applying it to an industrial pick-and-place unit (Figure 4) that performs repetitive movements between start point A with angular position $\theta_A = 0$ and endpoint B with angular position $\theta_B = 173.6°$. The resulting inertia $J(\theta)$ and load torque $\tau_l(\theta)$ profiles are presented in Figure 5. Because of the machine position limits θ_A and θ_B, only the green shaded part of the system properties is relevant during operation.

3.2. Viscous friction coefficient

Once the system properties $J(\theta)$ and $\tau_l(\theta)$ are determined, the only indefinite term in Equation (1) is the friction torque τ_f, and more specifically μ_v. In the previous description of the energy flows, the friction torque τ_f was neglected, leading to a simple objective (i.e. τ_{rms}) to quantify the energy consumption. However, it is important to verify this statement for the intended setup. Therefore this section describes a method to quantify the frictional forces τ_f.
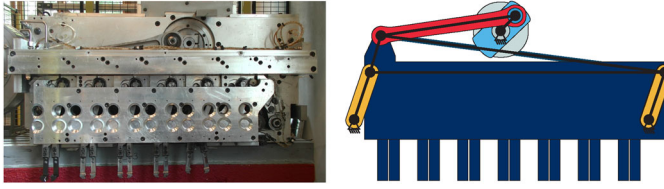
Figure 4. Experimental set-up (left) and schematic overview (right) of the pick- and place unit.
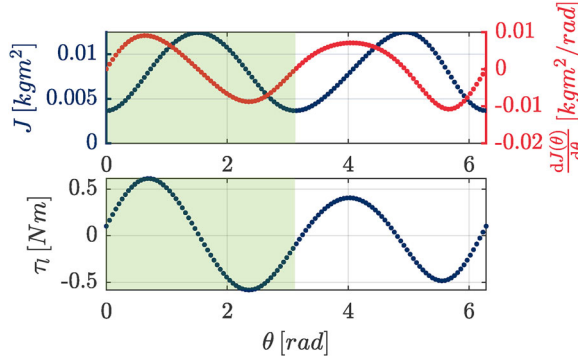

Figure 5. Values of system properties inertia $J(\theta)$ and load torque $\tau_l(\theta)$.

Since the viscous friction coefficient μ_v parameter is highly dependent on the practical setup, it is often only possible to determine this parameter experimentally. Therefore, a first measurement is carried out by using an arbitrary motion profile $\theta^*(t)$ as a set point and recording the resulting actual motor torque $\tau_{m;meas}(t)$ and position $\theta_{meas}(t)$. The arbitrary motion profile $\theta^*(t)$ can be determined by using a default motion profile such as a trapezoidal or s-curve profile.

After this measurement, a least squares fit can be used to determine the experimental value of μ_v, by fitting the torque model $\tau_m(\theta_{meas}(t), \mu_v)$ with the measured motor torque $\tau_{m;meas}$.

However, using the measured position θ_{meas} and its time derivatives $\dot{\theta}_{meas}, \ddot{\theta}_{meas}$ in the torque Equation (1) leads to unfeasible results since the derivatives amplify any noise that is present in the measurement. Therefore, the measured position $\theta_{meas}(t)$ is fitted with an n-th degree polynomial $\theta_{fit}(t) = \sum_{i=1}^{n} a_i t^i$ and is differentiated symbolically to smooth out any noise.

The friction parameter μ_v is thus determined by comparing the measured torque $\tau_{m;meas}(t)$ with the torque model and fitted motion profile $\tau_m(\theta_{fit}(t))$:

$$\underset{\mu_v \in \mathbb{R}}{\text{minimize}} \quad ||\tau_{m;meas}(t) - \tau_m(\theta_{fit}(t), \mu_v)||_2. \tag{9}$$

For the pick-and-place unit, a 13-th degree polynomial was fitted to the position and a viscous damping coefficient of 0.0157 Nms/rad was found. In Figure 6, a comparison of the measured $\tau_{m;meas}(t)$ and calculated $\tau_m(\theta_{fit}(t))$ torque is presented. The difference between the virtual torques (with and without friction) is minimal, which indicates that the friction can be neglected for the present case. The graph also shows a close correlation between the virtual and measured torque, which indicates that the virtual model can be effectively used to minimize the RMS torque τ_{rms} and, by extension, the energy consumption E.

4. Optimization approach

4.1. Motion Profile definition & rescaling

In this paper, a Chebyshev polynomial $\sum_{i=0}^{n} p_i T_i(x)$ is used to define the position profile $\theta(t)$, where $t \in [t_A, t_B]$, in between the start $(\theta(t_A) = \theta_A)$ and endpoint $(\theta(t_B) = \theta_B)$ of the motion
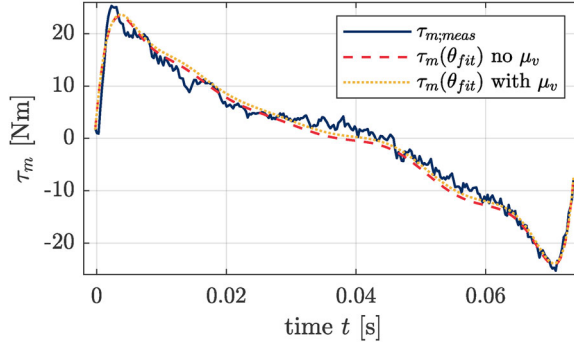
Figure 6. Comparison of the virtual $\tau_m(\theta^p(t))$ and measured torque $\tau_m^e(t)$ (with and without friction).

task. The sequence of orthogonal Chebyshev polynomials $T_k(x) = T_k(\cos(\vartheta))$, defined on the interval $x \in [-1, 1]$, is obtained from the recurrence relation:

$$\begin{aligned} T_0(x) &= 1, \quad T_1(x) = x, \\ T_{k+1}(x) &= 2xT_k(x) - T_{k-1}(x), \end{aligned} \tag{10}$$

Alternatively, the polynomials can be derived from the trigonometric definition, which gives exactly the same results:

$$T_k(x) = T_k(\cos(\vartheta)) = \cos(k\vartheta). \tag{11}$$

To use $T_n(x)$ as a representation for the position profile, a linear transformation from t into the range $[-1, 1]$ of x is required (Thompson 1994):

$$t = \frac{1}{2}(t_B - t_A)x + \frac{1}{2}(t_B + t_A) = ax + b, \tag{12}$$

where scale factors a and b are defined for the purpose of the following paragraphs. In addition, the position $\theta \in [\theta_A, \theta_B]$ is also rescaled to the interval $\phi \in [-1, 1]$, which makes it possible to obtain strict bounds on the design space in (32). Thus, the rescaled motion profile description $\phi(x)$ of degree n with optimizable coefficients $\mathbf{p} = [p_0, p_1, ..., p_n]^T$ is obtained:

$$\phi(x) = \sum_{i=0}^{n} p_i T_i(x), \quad x \in [-1, 1]. \tag{13}$$

The output of the motion simulations in the previous section deliver n_s samples of inertia $\mathbf{J} = [J_1, ..., J_{n_s}]^T$, load torque $\boldsymbol{\tau}_l = [\tau_{l,1}, ..., \tau_{l, n_s}]^T$ and corresponding angle query points $\boldsymbol{\theta} = [\theta_1, ..., \theta_{n_s}]^T$. Due to the position rescaling of the motion profile $\phi(x)$, the angle query points $\boldsymbol{\theta}$ have to be rescaled accordingly:

$$\boldsymbol{\phi} = \frac{2}{(\theta_B - \theta_A)} \boldsymbol{\theta} - \frac{(\theta_B + \theta_A)}{(\theta_B - \theta_A)} = c \, \boldsymbol{\theta} + d. \tag{14}$$

Moreover, as the property description is now defined on the rescaled interval $\phi \in [-1, 1]$, the following relationship holds with regard to the derivative properties such inertia variation $\frac{dJ(\phi)}{d\phi}$:

$$\frac{dJ(\phi)}{d\phi} = \frac{1}{2}(\theta_B - \theta_A)\frac{dJ(\theta)}{d\theta} = e \, \frac{dJ(\theta)}{d\theta}. \tag{15}$$

When using the rescaled position profile $\phi(x)$, it is important to rescale the torque from Equation (1) as well. Otherwise, the resulting values of the torque profile $\tau(x)$ are distorted which results in different objective values (i.e. τ_{rms}) and solutions. To preserve the motor torque's absolute values, the following rescaled torque equation is introduced:
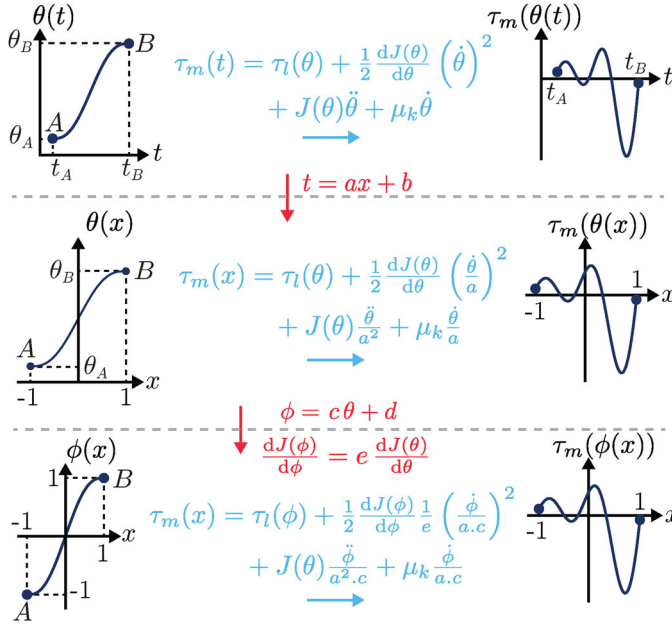
Figure 7. Original $\theta(t)$ and rescaled position profiles $\theta(x)$, $\phi(x)$ with their corresponding torque equations.

$$\tau_m(x) = \tau_l(\phi) + \frac{1}{2}\frac{\mathrm{d}J(\phi)}{\mathrm{d}\phi}\frac{1}{e}\left(\frac{\dot{\phi}}{a.c}\right)^2 + J(\theta)\frac{\ddot{\phi}}{a^2.c} + \mu_v\frac{\dot{\phi}}{a.c}. \tag{16}$$

An overview of the position and torque rescalings is presented in Figure 7. The new system Equation (16) ensures the system dynamics are equally scaled and the minima are not altered.

For what concerns the constraints, the rest-to-rest motion requires zero speed $\dot{\phi}$ and acceleration $\ddot{\phi}$ in the start and endpoint:

$$\begin{aligned}\phi(-1) &= -1, & \dot{\phi}(-1) &= 0, & \ddot{\phi}(-1) &= 0, \\ \phi(1) &= 1, & \dot{\phi}(1) &= 0, & \ddot{\phi}(1) &= 0.\end{aligned} \tag{17}$$

Referring to (13), and by incorporating the motion profile constraints (17), the lower degree coefficients $[p_0, ..., p_5]^T$ can be written as a function of the remaining coefficients $[p_6, ..., p_n]^T$, such that $n-5$ degrees of freedom (DOF) are kept available for the optimization algorithm (Hsu, Huang, and Fung 2014). Thus, the energy optimal motion profile problem is formulated as the following minimization problem with design variable vector $\mathbf{o} = [p_6, ..., p_n]^T$:

$$\underset{\mathbf{o}\in\mathbb{R}^{n-5}}{\text{minimize}} \qquad \tau_{rms} = \sqrt{\frac{1}{2}\int_{-1}^{1}\tau_m(\phi(x,\mathbf{o}))^2 \,\mathrm{d}x}. \tag{18}$$

In some applications, an additional constraint of zero jerk in the begin and endpoint can be imposed to limit the vibrations:

$$\dddot{\phi}(-1) = 0 \quad ; \quad \dddot{\phi}(1) = 0. \tag{19}$$

Because of these two extra equations, the DOF is reduced to $n-7$ and the design variable vector can be expressed as $\mathbf{o} = [p_8, ..., p_n]^T$.

4.2. Initialization & design space

In this paper, the resulting optimization problem is solved with both a fast *gradient-based* solver, the BFGS (Broyden–Fletcher–Goldfarb–Shanno) quasi-Newton method (Nocedal and Wright 2006), and a global heuristic solver, the *genetic algorithm* (Holland 1992).

For gradient-based optimization, a starting point needs to be defined. The use of the Chebyshev basis $T_i(x)$ in representation (13) allows initializing the optimization parameter vector at zero since the coefficients in a convergent Chebyshev series development of the motion profile function $\phi(x)$ would converge to zero (Majidian 2017). Here, we can safely assume some similar behavior for the coefficients p_i in (13).

For what concerns the genetic algorithm, a similar approach is used for the initialization of the population. However, because a GA often samples a wide part of the design space (Wenzhong and Porandla 2005), it is beneficial to determine the exact bounds on the design vector **o**. By doing so, the solver can cover a large part of the design space and reveal the global optimal solution. In the following paragraphs, thanks to the rescaled Chebyshev motion profile $\phi(x)$, strict bounds on the design vector **o** can be derived.

To define these bounds, we take a look at the projection of the position profile $\phi(x)$ onto the orthogonal Chebyshev polynomial basis $T_l(x)$. Given that $x = \cos(\theta)$, we introduce the inner product F:

$$
\begin{aligned}
F = \langle \phi(x), T_l(x) \rangle &= \int_{-1}^{1} \frac{\phi(x)T_l(x)}{\sqrt{1-x^2}} \ \mathrm{d}x \\
&= \int_{0}^{2\pi} \phi(\cos\theta)T_l(\cos\theta) \ \mathrm{d}\theta.
\end{aligned}
\tag{20}
$$

Then, by taking into account the position function definition (13), we find the following result:

$$
\begin{aligned}
F &= \int_{0}^{2\pi} \left(\sum_{k=0}^{n} p_k T_k(\cos\theta) \right) T_l(\cos\theta) \ \mathrm{d}\theta \\
&= \sum_{k=0}^{n} p_k \int_{0}^{2\pi} T_k(\cos\theta) T_l(\cos\theta) \ \mathrm{d}\theta.
\end{aligned}
\tag{21}
$$

Here, the integral $I = \int_{0}^{2\pi} T_k(\cos\theta)T_l(\cos\theta) \ \mathrm{d}\theta$ can be further simplified by using the Chebyshev polynomial orthogonality properties, which are rederived here for the sake of readability. Because of Equation (11) and by using the inverse Simpson rule of trigonometry, the integral I can be written as:

$$
\begin{aligned}
I &= \int_{0}^{2\pi} \cos(k\theta)\cos(\ell\theta) \ \mathrm{d}\theta \\
&= \frac{1}{2} \int_{0}^{2\pi} \cos((k+\ell)\theta) \ \mathrm{d}\theta + \frac{1}{2} \int_{0}^{2\pi} \cos((k-\ell)\theta) \ \mathrm{d}\theta.
\end{aligned}
\tag{22}
$$

This integral can be split into three cases:

1. $k = \ell = 0$

$$I = 2\pi, \tag{23}$$

2. $k = \ell \neq 0$

$$I = \pi, \tag{24}$$

3. $k \neq \ell$

$$I = 0. \tag{25}$$

Thus, by taking into account (25), only the term for which $k = l$ remains in the summation F:

$$F = p_\ell \int_0^{2\pi} \cos^2(\ell\theta) \ \mathrm{d}\theta. \tag{26}$$

This can be split into two cases. For $\ell = 0$ and by making use of (23) and (20) we find:

$$p_0 = \frac{1}{2\pi} \int_0^{2\pi} \phi(\cos\theta) \ \mathrm{d}\theta, \tag{27}$$

and for $\ell > 0$, by making use of (24) and (20):

$$p_\ell = \frac{1}{\pi} \int_0^{2\pi} \phi(\cos\theta) \cos(\ell\theta) \ \mathrm{d}\theta. \tag{28}$$

For $\theta \in [0, 2\pi]$, $\cos\theta$ lies in interval $[-1, 1]$. Because of the position rescalings of the motion profile $\phi(x)$, the image $\phi(\cos\theta)$ also lies in the interval $[-1, 1]$. Thus, we find:

$$|p_0| \leq \frac{1}{2\pi} \int_0^{2\pi} |\phi(\cos\theta)| \ \mathrm{d}\theta \leq \frac{1}{2\pi} \int_0^{2\pi} \mathrm{d}\theta = 1. \tag{29}$$

and

$$|p_\ell| \leq \frac{1}{\pi} \int_0^{2\pi} |\phi(\cos\theta)|| \cos(\ell\theta)| \ \mathrm{d}\theta \leq \frac{1}{\pi} \int_0^{2\pi} |\cos(\ell\theta)| \ \mathrm{d}\theta. \tag{30}$$

To calculate this last integral, we use the periodicity of the function $\cos(\ell\theta)$. This function has a period of $2\pi/\ell$, so goes ℓ times up and down on the interval $[0, 2\pi]$. So, after taking the absolute value of this function, we find 2ℓ times the integral over the positive part of a period, for example, the interval $[-\pi/2\ell, \pi/2\ell]$:

$$\frac{1}{\pi} \int_0^{2\pi} |\cos(\ell\theta)| \ \mathrm{d}\theta = \frac{2\ell}{\pi} \int_{-\pi/2\ell}^{\pi/2\ell} \cos(\ell\theta) \ \mathrm{d}\theta = \frac{4}{\pi}. \tag{31}$$

Thus, the following bounds for the coefficients p_i are obtained

$$|p_0| \leq 1 \quad \text{and} \quad |p_\ell| \leq \frac{4}{\pi}, \quad \ell = 1, ..., n. \tag{32}$$

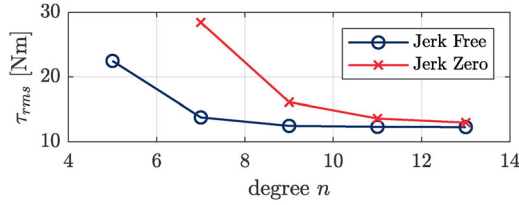These constraints on the design space simplify the subsequent optimization.

Figure 8. Results of the motion profile optimization for different degrees n.

5. Results

5.1. Motion Profile optimization

In order to assess the performance of the proposed method, a set of optimizations has been performed on the industrial pick-and-place unit depicted in Figure 4. The mechanism is required to move between its start position θ_A of 0° and end position θ_B of 173.6° and has a motion time Δt of $73.5ms$. As for the constraint, two different cases are considered, namely

- *Jerk Free (JF)*: Only the boundary constraints of (17) are taken into account. The corresponding rescaled Chebyshev position profile $\phi(x)$ of degree n is hereafter referred to as *cheb"n"*. A 5th-degree polynomial, hereafter indicated as *poly5*, is taken as the reference motion profile for comparison purposes. This is the smallest degree polynomial that satisfies the constraints.
- *Jerk Zero (J0)*: In addition to the constraint of a jerk-free optimization, a zero-jerk constraint is added in the start, and endpoint (19) is added to the motion profile definition. The resulting n-th degree position profile $\phi(x)$ is referred to as *cheb"n"J0*. The reference motion profile is in this case a 7th-degree polynomial, hereafter referred to as *poly7J0*.

For every case, the resulting optimization problem is solved in a MATLAB environment for degrees $n = 7, 9, 11,$ and 13. The results are presented in Figure 8 and Tables 1 and 2 where for every motion profile, the corresponding RMS torque τ_{rms} and solve time t_{sol} are displayed. Savings up to 54.4% are obtained in under 0.77 s. The results clearly converge toward a minimal value for increasing degree n. In general, the motion profiles which include the jerk constraint (19), have slightly bigger τ_{rms} values, which is to be expected due to the fact that this extra constraint limits the acceleration near the endpoints while it is desirable to have high accelerations here since the inertia is low.

In Table 1, the τ_{rms} values of a conventional trapezoidal 1/3 motion profile are presented as well, which accelerates during 1/3rd of the time, moves at a constant speed during 1/3rd, and decelerates at the last 1/3rd (Park, 1996). What is interesting in this table is that the torque demand can already be significantly reduced by selecting an adequate default motion law. Notwithstanding that the greatest savings are realized after optimization.

It is worth noting that for the jerk-free motion profiles, the same solution was found for both the genetic algorithm and gradient-based solver. However, the calculation times with GA are considerably higher. When including the jerk constraint, the GA comes close but does not completely reveal the full optimization potential. Therefore, for what concerns the present study, gradient-based optimizations algorithms are preferable. Since the GA did not obtain a better solution for any motion profile in the bounded search space, we can expect that the results obtained with the gradient-based method are global optimal solutions.

Although only the forward motion is considered here, similar results can be obtained for the return motion by simply changing the position constraints.

Table 1. Results of the motion profile optimization (Jerk Free).

	Gradient-based		Genetic algorithm	
JF	τ_{rms} [Nm]	t_{sol} [s]	τ_{rms} [Nm]	t_{sol} [s]
poly5 (ref.)	22.48	–	22.48	–
trap	$17.16 - 23.7\%$	–	$17.16 - 23.7\%$	–
cheb7	$13.78 - 38.7\%$	0.21	$13.78 - 38.7\%$	3.28
cheb9	$12.47 - 44.5\%$	0.32	$12.47 - 44.5\%$	40.33
cheb11	$12.33 - 45.2\%$	0.51	$12.33 - 45.2\%$	67.05
cheb13	$12.29 - 45.4\%$	1.06	$12.29 - 45.4\%$	142.34

Table 2. Results of the motion profile optimization (Jerk 0).

	Gradient-based		Genetic algorithm	
J0	τ_{rms} [Nm]	t_{sol} [s]	τ_{rms} [Nm]	t_{sol} [s]
poly7J0 (ref.)	28.44	–	28.44	–
cheb9J0	$16.12 - 43.3\%$	0.27	$16.12 - 43.3\%$	6.15
cheb11J0	$13.61 - 52.2\%$	0.38	$14.11 - 50.4\%$	175.23
cheb13J0	$12.98 - 54.4\%$	0.77	$13.15 - 53.8\%$	195.02
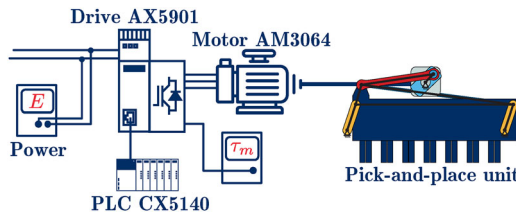
Figure 9. Schematic overview of the experimental setup.
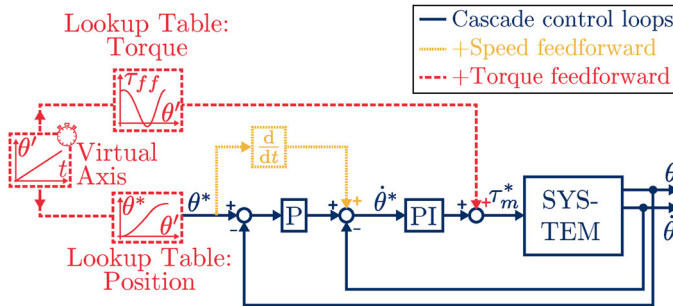
Figure 10. Schematic overview of the cascade motion controller with feedforward (Van Oosterwyck et al. 2019).

5.2. Measurements

The theoretical results are validated against experimental measurements on the pick-and-place unit (Figure 4). The setup comprises a Beckhoff CX5140 PLC, a Beckhoff AX5901 motor drive, and a Beckhoff AM3064 PMSM, which is connected to the shaft of the mechanism. In order to measure the input electrical energy, a Tektron PA4000 power analyzer is used to analyze the power supply (Figure 9).

The theoretical savings potential of the motion profile optimization is only fulfilled when the motor is capable of following the optimized position setpoint. Therefore, a performant motion controller needs to be designed in order to keep the tracking error as low as possible. Here, similar to (Van Oosterwyck et al. 2019), a cascade controller with torque and speed feedforward is

Table 3. Experimental results with energy measurement (Jerk Free).

JF	τ_{rms} [Nm]	$\tau_{rms;meas}$ [Nm]	E_{meas} [Wh]
poly5	22.48	19.59	312.2
trap	17.16 − 23.7%	15.88 − 18.98%	215.1 − 31.1%
cheb7	13.78 − 38.7%	13.40 − 31.6%	181.7 − 41.8%
cheb9	12.47 − 44.5%	12.07 − 38.4%	152.3 − 51.2%
cheb11	12.33 − 45.2%	11.93 − 39.1%	150.1 − 51.9%
cheb13	12.29 − 45.4%	11.83 − 39.6%	148.2 − 52.5%

Table 4. Experimental results with energy measurement (Jerk Zero).

J0	τ_{rms} [Nm]	$\tau_{rms;meas}$ [Nm]	E_{meas} [Wh]
poly7J0	28.44	25.30	458.5
cheb9J0	16.12 − 43.3%	15.81 − 37.5%	222.9 − 51.4%
cheb11J0	13.61 − 52.2%	13.08 − 48.3%	170.3 − 62.9%
cheb13J0	12.98 − 54.4%	12.72 − 49.7%	170.8 − 62.7%

employed as it has proven to be successful for high dynamic systems. The look-up table for the feedforward torque is determined using the torque from Equation (1) (Figure 10).

In Tables 3 and 4, the results of both the measured RMS torque $\tau_{rms;meas}$ and measured input electrical energy E_{meas} for different motion profiles are presented. As expected from the simulations, the lowest absolute energy consumption is obtained when using jerk-free motion profiles. When the jerk constraint is active, a decrease of 62.9% in energy consumption can be achieved by optimizing the motion profile, while a relative saving of 52.5% is possible if no extra constraint on the jerk is imposed.

The measured $\tau_{rms;meas}$ and calculated RMS motor torque τ_{rms} show a very high similarity, which confirms that the present system model is valid.

6. Conclusion

This study proposes a novel approach for motion profile optimization of PTP motions with Chebyshev polynomials. At first, system properties have been extracted from both CAD motion simulations and measurements to obtain an accurate virtual twin of the system. A Chebyshev motion profile with scaling laws is presented. Especially novel in this paper is the derivation of the boundary conditions of this profile which enables to define bounds for the design variables. The latter allows to use an optimizer that is designed to obtain globally optimal solutions, i.e. genetic algorithm. In addition, the solutions are validated with fast gradient-based optimization algorithms. Finally, experimental optimization results have been considered to verify the feasibility of the proposed solutions.

The numerical results, achieved on an exemplary model, clearly show that large τ_{rms} savings of up to 53.8% can be achieved. In addition, it is shown that by employing Chebyshev polynomials for the motion profile, a fast gradient-based optimization can be effectively employed with solve times under 0.8 s. At last, the validation measurements show that similar savings are obtained on the real machine with a maximum energy reduction of 62.9%.

Due to the straightforward implementation of both the optimization itself and integration of the resulting motion profiles in the motor drive, the proposed method can be easily adopted in any existing configuration where the CAD is data available. Therefore, the proposed method is expected to have a beneficial impact on the energy usage of the envisaged PTP applications.

Nomenclature

θ, ϕ	arrays of standard and rescaled position CAD samples
Δt	motion time

J, **τ**$_l$	arrays of inertia and load torque CAD samples
p, **o**	coefficient and design variable vector
μ_v	viscous friction coefficient
$\phi, \dot{\phi}, \ddot{\phi}, \dddot{\phi}$	rescaled motor position, speed, acceleration and jerk
τ_a, τ_v	acceleration and variation torque
τ_l, τ_f	load and frictional torque
$\tau_m, \tau_{m;meas}$	calculated and measured motor torque
$\tau_{rms}, \tau_{rms;meas}$	calculated and measured root-mean-square motor torque
$\theta, \dot{\theta}, \ddot{\theta}, \dddot{\theta}$	motor position, speed, acceleration and jerk
θ^*	setpoint position
θ_A, θ_B	start and end position
$\theta_{meas}, \theta_{fit}$	measured and fitted position
a, b, c, d, e	scaling constants
E, E_{meas}	calculated and measured electrical input energy
E_k, E_p, E_l	kinetic, potential and loss energy
i	current
J, J_m, J_l	total, motor and load inertia
k_v, k_t	back emf and motor torque constant
p	pole pairs
P_e	electric power
R	resistance
t, x	standard and rescaled time
t_A, t_B	start and end time
T_i	i-th Chebyshev polynomial
t_{sol}	solve time
u, ϵ	voltage and electric back emf

Funding

References

Baggetta, M., P. Bilancia, M. Pellicciari, and G. Berselli. 2021. An integrated approach for motion law optimization in partially compliant slider-crank mechanisms. In *2021 20th International Conference on Advanced Robotics, ICAR 2021*, 695–700. IEEE.

Berselli, G., F. Balugani, M. Pellicciari, and M. Gadaleta. 2016. Energy-optimal motions for servo-systems: A comparison of spline interpolants and performance indexes using a CAD-based approach. *Robotics and Computer-Integrated Manufacturing* 40:55–65. doi:10.1016/j.rcim.2016.01.003.

Betts, J. T. 1998. A survey of numerical methods for trajectory optimization. *Journal of Guidance, Control, and Dynamics* 21 (2):193–207. doi:10.2514/2.4231.

Biagiotti, L, and C. Melchiorri. 2021. Optimization of generalized S-curve trajectories for residual vibration suppression and compliance with kinematic bounds. *IEEE/ASME Transactions on Mechatronics* 26 (5):2724–34. doi:10.1109/TMECH.2020.3045504.

Bo, H. 2008. Electric Motors—Alignment of Standards and Best Practice Programmes with APEC. Final Report.

Boryga, M, and A. Graboś. 2009. Planning of manipulator motion trajectory with higher-degree polynomials use. *Mechanism and Machine Theory* 44 (7):1400–19. doi:10.1016/j.mechmachtheory.2008.11.003.

Boscariol, P., R. Caracciolo, D. Richiedei, and A. Trevisani. 2020. Energy optimization of functionally redundant robots through motion design. *Applied Sciences (Switzerland)* 10 (9):3022–13. doi:10.3390/app10093022.

Brancati, R., C. Rossi, and F. Timpone. 2007. Dynamic behavior and motion planning of a robot arm with non-rigid transmission. *Mechanics Based Design of Structures and Machines* 35 (4):347–62. doi:10.1080/15397730701606627.

Carabin, G, and L. Scalera. 2020. On the trajectory planning for energy efficiency in industrial robotic systems. *Robotics* 9 (4):89–13. doi:10.3390/robotics9040089.

Carabin, G, and R. Vidoni. 2021. Energy-saving optimization method for point-to-point trajectories planned via standard primitives in 1-DoF mechatronic systems. *The International Journal of Advanced Manufacturing Technology* 116 (1-2):331–4. doi:10.1007/s00170-021-07277-y.

Carabin, G., E. Wehrle, and R. Vidoni. 2017. A review on energy-saving optimization methods for robotic and automatic systems. *Robotics* 6 (4):39–21. doi:10.3390/robotics6040039.

Cheng, Q., W. Xu, Z. Liu, X. Hao, and Y. Wang. 2021. Optimal trajectory planning of the variable-stiffness flexible manipulator based on CADE algorithm for vibration reduction Control. *Frontiers in Bioengineering and Biotechnology* 9:766495–14. doi:10.3389/fbioe.2021.766495.

Chettibi, T., H. Lehtihet, M. Hadda, and S. Hanchi. 2004. Minimum cost trajectory planning for industrial robots. *European Journal of Mechanics—A/Solids* 23 (4):703–15. doi:10.1016/j.euromechsol.2004.02.006.

Delchev, K, and E. Zahariev. 2008. Computer simulation-based synthesis of learning-control law of robots. *Mechanics Based Design of Structures and Machines* 36 (3):225–48. doi:10.1080/15397730802275405.

Diehl, M., H. G. Bock, H. Diedam, and P.-B. Wieber. 2006. Fast direct multiple shooting algorithms for optimal robot control. In *Fast Motions in Biomechanics and Robotics: Optimization and Feedback Control*, eds. M. Diehl and K. Mombaur, 65–93. Berlin, Heidelberg: Springer Berlin Heidelberg.

Dresig, H, and F. Holzweißig. 2010. *Dynamics of machinery: Theory and applications*. Berlin Heidelberg: Springer.

Ellis, G. 2012. *Control system design guide* (4th ed.). Amsterdam: Elsevier.

Gadaleta, M., M. Pellicciari, and G. Berselli. 2019. Optimization of the energy consumption of industrial robots for automatic code generation. *Robotics and Computer-Integrated Manufacturing* 57:452–64. doi:10.1016/j.rcim.2018.12.020.

Gasparetto, A, and V. Zanotto. 2007. A new method for smooth trajectory planning of robot manipulators. *Mechanism and Machine Theory* 42 (4):455–71. doi:10.1016/j.mechmachtheory.2006.04.002.

Glodde, A, and M. Afrough. 2014. Energy efficiency evaluation of an underactuated robot in comparison to traditional robot kinematics. *Procedia CIRP* 23 (C):127–30. doi:10.1016/j.procir.2014.10.087.

Ha, J. L., R. F. Fung, K. Y. Chen, and S. C. Hsien. 2006. Dynamic modeling and identification of a slider-crank mechanism. *Journal of Sound and Vibration* 289 (4-5):1019–44. doi:10.1016/j.jsv.2005.03.011.

Holland, J. H. 1992. *Adaptation in natural and artificial systems: An introductory analysis with applications to biology, control and artificial intelligence*. Cambridge, MA, USA: MIT Press.

Hsu, Y. L., M. S. Huang, and R. F. Fung. 2014. Energy-saving trajectory planning for a toggle mechanism driven by a PMSM. *Mechatronics* 24 (1):23–31. doi:10.1016/j.mechatronics.2013.11.004.

Huang, J., P. Hu, K. Wu, and M. Zeng. 2018. Optimal time-jerk trajectory planning for industrial robots. *Mechanism and Machine Theory* 121:530–44. doi:10.1016/j.mechmachtheory.2017.11.006.

Kelly, M. P. 2017. Transcription methods for trajectory optimization: A beginners tutorial. *SIAM Review* 59 (4):849–904. doi:10.1137/16M1062569.

Kiel, E. 2008. *Drive solutions*. Berlin, Heidelberg: Springer.

Kuenzer, U, and M. L. Husty. 2016. Generation and optimal choice of joint trajectories using all solutions of inverse kinematics of general 6-R robots. *Mechanics Based Design of Structures and Machines* 44 (1-2):146–59. doi:10.1080/15397734.2016.1152192.

Lee, D, and C. W. Ha. 2020. 9) Optimization process for polynomial motion profiles to achieve fast movement with low vibration. *IEEE Transactions on Control Systems Technology* 28 (5):1892–901. doi:10.1109/TCST.2020.2998094.

Majidian, H. 2017. On the decay rate of Chebyshev coefficients. *Applied Numerical Mathematics* 113:44–53. doi:10.1016/j.apnum.2016.11.004.

Mezzadri, F, and E. Galligani. 2016. A Chebyshev technique for the solution of optimal control problems with nonlinear programming methods. *Mathematics and Computers in Simulation* 121:95–108. doi:10.1016/j.matcom.2015.08.023.

Nguyen, K. D., I. M. Chen, and T. C. Ng. 2007. Planning Algorithms for S-curve Trajectories. In *IEEE/ASME International Conference on Advanced Intelligent Mechatronics, AIM*, Volume 1, 1–6.

Nocedal, J, and S. Wright. 2006. *Numerical optimization* (2nd ed.). Berlin, Heidelberg: Springer Science & Business Media.

Park, J. S. 1996. Motion profile planning of repetitive point-to-point control for maximum energy conversion efficiency under acceleration conditions. *Mechatronics* 6 (6):649–63. doi:10.1016/0957-4158(96)00012-8.

Pellicciari, M., G. Berselli, and F. Balugani. 2015. On designing optimal trajectories for servo-actuated mechanisms: Detailed virtual prototyping and experimental evaluation. *IEEE/ASME Transactions on Mechatronics* 20 (5):2039–52. doi:10.1109/TMECH.2014.2361759.

Piazzi, A, and A. Visioli. 1998. Global minimum-time trajectory planning of mechanical manipulators using interval analysis. *International Journal of Control* 71 (4):631–52. doi:10.1080/002071798221713.

Rao, A. V. 2014. Trajectory optimization: A survey. In *Optimization in automotive control and optimal systems*, eds. H. Waschl, I. Kolmanovsky, M. Steinbuch, and L. del Re, Vo. 455. *Lecture Notes in Control and Information Sciences*, 3–18. Cham: Springer International Publishing.

Richiedei, D, and A. Trevisani. 2016. Analytical computation of the energy-efficient optimal planning in rest-to-rest motion of constant inertia systems. *Mechatronics* 39:147–59. doi:10.1016/j.mechatronics.2016.05.004.

Rizzoni, G, and J. Kearns. 2003. *Principles and applications of electrical engineering*. McGraw-Hill (London).

Shiller, Z. 1996. Time-energy optimal control of articulated systems with geometric path constraints. *Journal of Dynamic Systems, Measurement, and Control* 118 (1):139–43. doi:10.1115/1.2801134.

Sollmann, K., M. Jouaneh, and D. Lavender. 2010. Dynamic modeling of a two-axis parallel H-frame-type XY positioning system. *IEEE/ASME Transactions on Mechatronics* 15 (2):280–90. doi:10.1109/TMECH.2009.2020823.

Thompson, W. J. 1994. Chebyshev polynomials: After the spelling the rest is easy. *Computers in Physics* 8 (2):161. doi:10.1063/1.4823278.

Van Oosterwyck, N., A. Ben Yahya, A. Cuyt, and S. Derammelaere. 2020. CAD based trajectory optimization of PTP motions using Chebyshev polynomials. In 2020 IEEE/ASME International Conference on Advanced Intelligent Mechatronics (AIM), Boston, pp. 403–408. IEEE.

Van Oosterwyck, N., F. Vanbecelaere, M. Haemers, D. Ceulemans, K. Stockman, and S. Derammelaere. 2019. CAD enabled trajectory optimization and accurate motion control for repetitive tasks. In *2019 IEEE 15th International Conference on Control and Automation (ICCA)*, 387–92. Edinburgh: IEEE.

Vanbecelaere, F., N. Van Oosterwyck, S. Derammelaere, A. Cuyt, M. Monte, and K. Stockman. 2022. On-line motion profile optimization for reciprocating mechanisms. *Mechanism and Machine Theory* 173:104833. doi:10.1016/j.mechmachtheory.2022.104833.

Vanbecelaere, F., S. Derammelaere, N. Nevaranta, J. De Viaene, F. Verbelen, K. Stockman, and M. Monte. 2020. Online tracking of varying inertia using a SDFT approach. *Mechatronics* 68:102361. doi:10.1016/j.mechatronics.2020.102361.

Vlassenbroeck, J, and R. Van Dooren. 1988. A Chebyshev technique for solving nonlinear optimal control problems. *IEEE Transactions on Automatic Control* 33 (4):333–40. doi:10.1109/9.192187.

Walsch, H., I. Kolmanovsky, M. Steinbuch, and L. del Re. 2014. *Optimization and optimal control in automotive systems*, Vol. 455. *Lecture Notes in Control and Information Sciences*. Cham: Springer International Publishing.

Wenzhong, G, and S. K. Porandla. 2005. Design optimization of a parallel hybrid electric powertrain. 2005 IEEE Vehicle Power and Propulsion Conference, *VPPC 2005*, 530–535. doi:10.1109/VPPC.2005.1554609.

Westphal, L. C. 2001. *Handbook of control systems engineering*. Springer US.

Wu, Z., J. Chen, T. Bao, J. Wang, L. Zhang, and F. Xu. 2022. A novel point-to-point trajectory planning algorithm for industrial robots based on a locally asymmetrical jerk motion profile. *Processes* 10 (4):728–18. doi:10.3390/pr10040728.